Pressure and Temperature Dependence of the Recombination of *p*-Fluorobenzyl Radicals

Changyoul Lee, Klaus Luther, Kawon Oum,* and Jürgen Troe

Institut für Physikalische Chemie, Universität Göttingen, Tammannstrasse 6, D-37077 Göttingen, Germany

Received: November 30, 2005; In Final Form: January 7, 2006

The rate constants of the recombination reaction of *p*-fluorobenzyl radicals, *p*-F−$C_6H_4CH_2$ + *p*-F−$C_6H_4CH_2$ (+M) → $C_{14}H_{12}F_2$ (+M), have been measured over the pressure range 0.2−800 bar and the temperature range 255−420 K. Helium, argon, and CO_2 were employed as bath gases (M). At pressures below 0.9 bar in Ar and CO_2, and 40 bar in He, the rate constant k_1 showed no dependence on the pressure and the nature of the bath gas, clearly indicating that it had reached the limiting high-pressure value of the energy-transfer (ET) mechanism ($k_{1,\infty}^{ET}$). A value of $k_{1,\infty}^{ET}(T) = (4.3 \pm 0.5) \times 10^{-11}$ $(T/300\ \mathrm{K})^{-0.2}$ cm^3 molecule^{-1} s^{-1} was determined. At pressures above about 5 bar, the k_1 values in Ar and CO_2 were found to gradually increase in a pressure range where according to energy-transfer mechanism, they should remain at the constant value $k_{1,\infty}^{ET}$. The enhancement of the recombination rate constant beyond the value $k_{1,\infty}^{ET}$ increased in the order He < Ar < CO_2, and it became more pronounced with decreasing temperature. The dependences of k_1 on pressure, temperature, and the bath gas were similar to previous observations in the recombination of benzyl radicals. The effect of fluorine-substitution of the benzyl ring on k_1 values is discussed. The present results confirm the significant role of radical complexes in the recombination kinetics of benzyl-type radicals in the gas−liquid transition range. The observations on a rate enhancement beyond the experimental value of $k_{1,\infty}^{ET}$ at elevated densities up to the onset of diffusion-control are consistently explained by the kinetic contribution of a "radical-complex" mechanism which is solely based on standard van der Waals interaction between radicals and bath gases.

1. Introduction

The pressure dependence of recombination reactions reflects the important influence of the surrounding bath medium on the dynamics of these processes. Collisional energy transfer in low-pressure gases and molecular diffusion at the high densities of liquid solutions are the well understood extremes of the rate-limiting intermolecular interactions in radical combination kinetics. However, in the intermediate regime between high-density gases and liquids, under the often very interesting conditions of supercritical fluids, the superposition of various reagent-solvent interactions is not yet well understood.[1,2] In this range, van der Waals complexes may play a role in the reaction mechanism and influence the rate constant.

In several studies of recombination reactions over wide pressure ranges (0.01−1000 bar) and in the temperature range 200−400 K, we have found unexpected "high-pressure" behavior. An enhancement of the rate constant above the experimentally established "high-pressure limit" of a standard energy-transfer (ET) mechanism was observed. The ET mechanism is represented by a scheme with association, dissociation, and collisional energy transfer steps

$$\mathrm{A + B \rightarrow AB^*}$$
$$\mathrm{AB^* \rightarrow A + B}$$
$$\mathrm{AB^* + M \rightarrow AB + M}$$

where A and B denote radicals or molecules and M is the solvent species. The experimentally observed enhancement of the recombination rate constant beyond the value given by this scheme varies markedly with the nature of the bath medium and shows strong negative temperature dependence. We have consistently interpreted the experimental phenomena, including bath-gas and temperature dependence in terms of a radical-complex (RC) mechanism, i.e., a mechanism following the scheme

$$\mathrm{A + M \rightarrow AM}$$
$$\mathrm{AM \rightarrow A + M}$$
$$\mathrm{AM + B \rightarrow AB + M}$$

taking into account the nature and density-dependent concentration of the weakly bound reagent-solvent van der Waals complexes.[3,4] The RC mechanism has been known for a long time, but indications for its presence and discussions of its relative importance have always been limited to small systems like atomic recombination,[5] ozone formation,[6,7] or ultralow temperatures.[8] Our recent search for RC dynamics for large radicals has the advantage that it avoids complications from the pressure dependence in the falloff regime of the ET mechanism, which extends to very high pressures for atoms or small radicals. For large radicals like those studied in the present work, the limiting "high-pressure" rate constant of the energy-transfer mechanism (k_∞^{ET}) is established far below 1 bar and truly constant k_∞^{ET} are measured over a broad density range before the additional pressure dependence of the rate constant is observed. To prove that contributions of the RC-mechanism are to be expected quite generally in combination reactions, it is necessary to find additional experimental evidence.

In this work, we present a new example for the RC mechanism. The recombination reaction of *p*-fluorobenzyl

* Corresponding author. Telephone: +49 551 39 12598. Fax: +49 551 39 3150. E-mail: koum@gwdg.de.

10.1021/jp056944y CCC: $33.50
Published on Web 02/07/2006

radicals was investigated in order to see if the enhancement of recombination rate constants at high pressures can also be found in this system and, if this is the case, to quantify the effect of fluorine substitution of the benzyl ring. The rate constants of the combination reaction

$$p\text{-F}-C_6H_4CH_2 + p\text{-F}-C_6H_4CH_2\ (+M) \rightarrow C_{14}H_{12}F_2\ (+M) \quad k_1 \quad (1)$$

have been measured over the pressure range 0.2−800 bar and the temperature range 255−420 K. Helium, argon, and CO_2 were employed as the bath gases (M). To our knowledge, there has been no direct measurement of reaction 1 in the gas-phase so far. Devolder and co-workers have investigated reaction rates of *p*- and *m*-fluorobenzyl radicals with O_2, NO, and NO_2 by discharge flow/laser-induced fluorescence experiments in the gas-phase.[9,10] However, the self-combination reaction of fluorobenzyl radicals was irrelevant in these studies. On the other hand, there were numerous spectroscopic studies of *p*-fluorobenzyl radicals in the visible region (absorption and fluorescence spectra, fluorescence lifetime), because the fluorine substituted aromatic compounds emit stronger fluorescence than other halogenated aromatic compounds.[11−15] However, no direct study of the absorption band of *p*-fluorobenzyl radicals in the UV region is available. In the following, we present our results which provide another example for a significant contribution of the radical-complex mechanism in the gas−liquid transition region. In addition, we investigate the transient UV absorption spectrum of *p*-fluorobenzyl radicals.

2. Experimental Section

Our experimental set up has been described in detail before, and only the main features are mentioned here.[16,17] The experiments were carried out in a temperature-controlled high-pressure optical flow cell. Gas-phase *p*-fluorobenzyl radicals were generated by excimer laser photolysis of Cl_2 at 308 nm and subsequent H-abstraction by the resulting Cl atoms from *p*-fluorotoluene. Mixtures of Cl_2, *p*-fluorotoluene, and the bath gas were compressed in an oil-free diaphragm compressor, and then were allowed to flow through the high-pressure cell (path length 10 cm, optical diameter 0.9 cm). For experiments at pressures below 1 bar, a flow cell made of glass was used (path length: 51 cm optical diameter 3 cm). Flow rates were controlled by flow meters such that reagents and products were removed from the observation volume between the laser pulses. Absorption−time profiles at 253 nm, on time scales of microseconds to milliseconds, were detected by a prism-monochromator photomultiplier arrangement with a bandwidth of 2 nm and recorded in a digital storage oscilloscope. Typically several hundred shots were averaged, which allowed us to monitor the progress of reaction 1. The light source for the absorption measurements was a high-pressure Hg−Xe lamp. The bath gases helium, argon, and CO_2 were of a purity higher than 99.998%. Residual impurities in the bath gases, especially oxygen, were carefully removed by a series of gas cleaning adsorbers and dust filters. The reagent grade *p*-fluorotoluene was from Aldrich and was purified in a pump−thaw−freezing cycle prior to use.

Possible systematic errors present in the experiments are probably small. Systematic drifts in the temperature and pressure measurements were negligible. Uncertainties in the concentrations of reactants and bath gases due to wall adsorption/desorption were minimized by allowing complete mixing overnight. Depositions on the windows, which might cause changes in the absorption signals, are largely avoided by the specific construction of the high-pressure cell, where the flow of the mixture is passing close to both window surfaces allowing an efficient exchange.

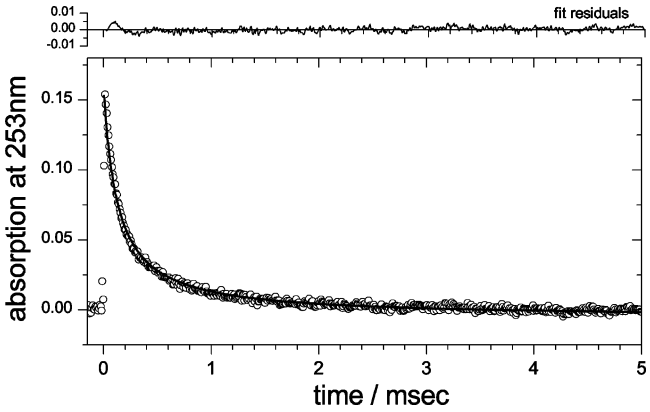

Figure 1. *p*-Fluorobenzyl absorption signals at 253 nm, recorded after the photolysis at 308 nm of mixtures of 1.9 mbar of Cl_2, 9.8 mbar of *p*-fluorotoluene and 800 bar of argon at 300 K: (○) experimental data; (solid line) fit (see text); upper trace, the residual of the fit.

3. Results

3.1. Absorption—Time Profiles at 253 nm. Following our previously established approach,[16,18] *p*-fluorobenzyl radicals were generated by the laser flash photolysis of Cl_2 at 308 nm and the subsequent reaction of chlorine atoms with excess *p*-fluorotoluene

$$Cl_2 + h\nu\ (308\ \text{nm}) \rightarrow 2\ Cl \quad (2)$$

$$Cl + p\text{-F}-C_6H_4CH_3 \rightarrow p\text{-F}-C_6H_4CH_2 + HCl \quad (3)$$

Reaction 3 proceeds analogous to the H-abstraction from toluene by Cl atoms, and we assume that reaction 3 is the only channel, such as that known for the Cl + toluene reaction,[19] and that k_3 is similarly large as k(Cl + toluene) = 6×10^{-10} cm^3 molecule^{-1} s^{-1}.[20] Under our conditions, Cl atoms then are instantly and stoichiometrically converted to *p*-fluorobenzyl radicals. Typical concentrations were $[Cl]_0$ (=[*p*-fluorobenzyl]$_0$) = (1−5) $\times 10^{13}$ molecules cm^{-3} and [*p*-fluorotoluene] = (0.7−7) $\times 10^{16}$ molecules cm^{-3}.

Figure 1 shows a typical absorption−time profile of *p*-fluorobenzyl radicals at 253 nm in 800 bar of Ar at 300 K. All absorption−time profiles showed the instant increase of the *p*-fluorobenzyl concentrations, which then was followed by a clean second-order decay entirely assignable to reaction 1. The residuals of the fits did not show any systematic deviations, giving additional support to the reported values of k_1. Table 1 summarizes the measured k_1 values from our work.

3.2. λ- and *T*-Dependent Absorption Coefficients of *p*-Fluorobenzyl Radicals. Because of the second-order nature of reaction 1, the measured reaction rates are sensitive to the initial concentration of *p*-fluorobenzyl radicals and, therefore, to the absorption coefficients $\sigma_{p-\text{fluorobenzyl}}$. Information on $\sigma_{p-\text{fluorobenzyl}}$ is not yet available in the literature. As a first step we, therefore, determined λ- and *T*-dependent values of $\sigma_{p-\text{fluorobenzyl}}(\lambda,T)$. With identical initial concentrations of the precursors Cl_2 and *p*-fluorotoluene, absorption−time profiles of *p*-fluorobenzyl radicals were measured at different detection wavelengths between 236 and 262 nm. The total pressure of argon was kept at 350 mbar. At each wavelength, the maximum absorption was obtained by extrapolating the absorption−time profile to zero

TABLE 1: Pseudo-Second-Order Rate Constants for the Combination Reaction of *p*-Fluorobenzyl Radicals (k_1)

(a) He Data at 300 K

p(He)[a]	[He][b]	k_1[c]	p(He)[a]	[He][b]	k_1[c]	p(He)[a]	[He][b]	k_1[c]	p(He)[a]	[He][b]	k_1[c]
0.2	4.83E18	4.3	3	7.23E19	4.2	10	2.40E20	4.3	43	1.02E21	4.4
0.4	9.65E18	4.4	4	9.64E19	4.3	15	3.60E20	4.6	200	4.42E21	5.4
0.6	1.45E19	4.4	5	1.20E20	4.4	20	4.78E20	4.6	300	6.36E21	5.0
0.8	1.93E19	4.5	7	1.68E20	4.2	25	5.97E20	4.1	400	8.15E21	4.4
0.9	2.17E19	4.4	10	2.40E20	4.5	30	7.14E20	4.5	500	9.82E21	5.1

(b) Ar Data at 300 K

p(Ar)[a]	[Ar][b]	k_1[c]	p(Ar)[a]	[Ar][b]	k_1[c]	p(Ar)[a]	[Ar][b]	k_1[c]	p(Ar)[a]	[Ar][b]	k_1[c]
0.39	9.45E18	4.4	4	9.68E19	5.3	80	2.01E21	5.2	600	1.16E22	1.9
0.49	1.19E19	4.4	5	1.21E20	5.4	100	2.53E21	5.5	700	1.25E22	2.2
0.69	1.67E19	4.5	7	1.70E20	5.4	200	5.06E21	4.1	800	1.33E22	2.3
0.79	1.91E19	4.6	10	2.43E20	6.2	300	7.27E21	3.3			
2	4.83E19	5.3	30	7.37E20	5.7	400	9.04E21	1.9			
3	7.25E19	5.0	50	1.24E21	6.4	500	1.04E22	2.7			

(c) CO_2 Data at 300 K

p(CO_2)[a]	[CO_2][b]	k_1[c]	p(CO_2)[a]	[CO_2][b]	k_1[c]	p(CO_2)[a]	[CO_2][b]	k_1[c]	p(CO_2)[a]	[CO_2][b]	k_1[c]
0.3	7.25E18	4.7	1	2.43E19	4.7	6	1.50E20	5.4	30	8.67E20	8.7
0.5	1.21E19	4.8	2	4.87E19	5.6	7	1.75E20	6.0	40	1.26E21	10.9
0.7	1.70E19	4.4	3	7.35E19	5.4	8	2.01E20	6.4	45	1.49E21	11.2
0.8	1.94E19	4.5	4	9.85E19	5.5	10	2.54E20	6.2	48	1.64E21	11.0
0.9	2.18E19	4.6	5	1.24E20	5.5	20	5.39E20	7.1			

(d) He Data near 5 bar

T/K	[He][b]	k_1[c]	T/K	[He][b]	k_1[c]	T/K	[He][b]	k_1[c]	T/K	[He][b]	k_1[c]
255	1.21E20	5.4	290	1.21E20	4.1	341	1.21E20	3.7	400	1.21E20	4.2
270	1.21E20	4.6	300	1.21E20	4.3	362	1.21E20	4.3	420	1.21E20	4.2
279	1.21E20	4.6	321	1.21E20	4.4	380	1.21E20	4.3			

(e) Ar Data near 5 bar

T/K	[Ar][b]	k_1[c]	T/K	[Ar][b]	k_1[c]	T/K	[Ar][b]	k_1[c]	T/K	[Ar][b]	k_1[c]
259	1.20E20	7.5	290	1.20E20	5.1	320	1.20E20	5.0	380	1.20E20	4.5
269	1.20E20	6.3	300	1.20E20	5.1	340	1.20E20	4.6	395	1.20E20	4.5
280	1.20E20	5.8	300	1.20E20	5.6	360	1.20E20	4.6			

(f) CO_2 Data at 5 bar

T/K	[CO_2][b]	k_1[c]	T/K	[CO_2][b]	k_1[c]	T/K	[CO_2][b]	k_1[c]
275	1.36E20	7.8	300	1.24E20	5.5	350	1.05E20	4.5

(g) CO_2 Data at 20 bar

T/K	[CO_2][b]	k_1[c]	T/K	[CO_2][b]	k_1[c]	T/K	[CO_2][b]	k_1[c]	T/K	[CO_2][b]	k_1[c]
259	5.39E20	13.1	300	5.39E20	7.2	340	4.56E20	5.9	400	3.76E20	4.9
279	5.39E20	8.9	300	5.39E20	7.0	360	4.25E20	5.5	420	3.55E20	4.9
290	5.39E20	7.9	320	4.93E20	6.5	380	3.99E20	5.7			

(h) CO_2 Data at 275 K

p(CO_2)[a]	[CO_2][b]	k_1[c]	p(CO_2)[a]	[CO_2][b]	k_1[c]	p(CO_2)[a]	[CO_2][b]	k_1[c]	p(CO_2)[a]	[CO_2][b]	k_1[c]
3	8.06E19	6.4	7	1.93E20	7.2	15	4.42E20	8.9	25	8.13E20	9.9
4	1.08E20	7.2	10	2.83E20	9.0	20	6.17E20	8.2	30	1.04E21	11.2
5	1.36E20	7.8									

(i) CO_2 Data at 350 K

p(CO_2)[a]	[CO_2][b]	k_1[c]	p(CO_2)[a]	[CO_2][b]	k_1[c]	p(CO_2)[a]	[CO_2][b]	k_1[c]	p(CO_2)[a]	[CO_2][b]	k_1[c]
2	4.16E19	4.2	7	1.48E20	4.8	10	2.13E20	4.4	30	6.83E20	7.0
5	1.05E20	4.5	8	1.69E20	5.1	20	4.40E20	5.6	40	9.44E20	7.8

(j) CO_2 Data at 400 K

p(CO_2)[a]	[CO_2][b]	k_1[c]	p(CO_2)[a]	[CO_2][b]	k_1[c]	p(CO_2)[a]	[CO_2][b]	k_1[c]	p(CO_2)[a]	[CO_2][b]	k_1[c]
2	3.63E19	4.3	6	1.10E20	4.0	20	3.76E20	4.6	40	7.81E20	5.0
4	7.30E19	4.2	8	1.47E20	4.3	30	5.74E20	5.7			

[a] Pressure of the bath gas, given in bar. [b] Density of the bath gas, given in molecules cm^{-3}. [c] Rate constant, given in 10^{-11} cm^3 $molecule^{-1}$ s^{-1}.

time, which was then corrected for the spectral response curve of the detection system and also for the laser energy. Figure 2 shows the resulting relative absorption spectrum of *p*-fluorobenzyl radicals. Structureless absorption bands were obtained and the maximum absorption was located at 256 nm. The spectral resolution of each data point in Figure 2 was 2 nm.

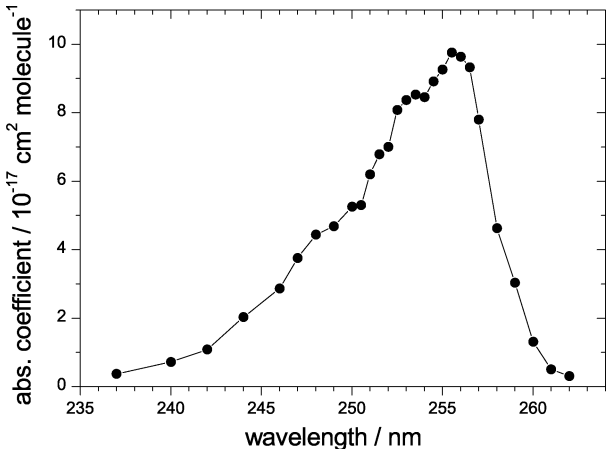

Figure 2. Absorption spectrum of *p*-fluorobenzyl radicals in 350 mbar Ar at 300 K.

TABLE 2: Absorption Coefficients of *p*-Fluorobenzyl Radicals, $\sigma_{p-\text{fluorobenzyl}}$, at 300 K

λ/nm	$\sigma_{p-\text{fluorobenzyl}}$[a]	λ/nm	$\sigma_{p-\text{fluorobenzyl}}$[a]	λ/nm	$\sigma_{p-\text{fluorobenzyl}}$[a]
237	0.4 ± 2.4	251	6.2 ± 0.9	256	9.6 ± 0.7
240	0.7 ± 2.1	251.5	6.8 ± 0.8	256.5	9.3 ± 0.8
242	1.1 ± 1.6	252	7.0 ± 0.9	257	7.8 ± 0.9
244	2.0 ± 1.2	252.5	8.1 ± 1.0	258	4.6 ± 1.0
246	2.9 ± 1.2	253	8.4 ± 1.0	259	3.0 ± 1.0
247	3.8 ± 1.2	253.5	8.5 ± 1.0	260	1.3 ± 1.0
248	4.4 ± 0.9	254	8.5 ± 0.7	261	0.5± 0.7
249	4.7 ± 1.0	254.5	8.9 ± 0.7	262	0.3 ± 0.8
250	5.3 ± 0.9	255	9.3 ± 0.7		
250.5	5.3 ± 0.9	255.5	9.8 ± 0.7		

[a] Absorption coefficients, given in 10^{-17} cm^2 molecule^{-1}.

To determine absolute absorption coefficients, the photolysis yield of Cl_2 in the cell has to be known such that the concentration of *p*-fluorobenzyl radicals can be determined: however, this measurement was found to be not easy to perform. In the present work, we decided instead to use benzyl radicals as a calibration source. First, we measured the absorption−time traces of benzyl radicals at 253 nm, produced in reaction 3 when toluene is employed instead of *p*-fluorotoluene. Then, under the same initial concentration of Cl_2 (and therefore $[Cl]_0$) and at the same laser intensity, absorption−time traces of *p*-fluorobenzyl radicals were measured. Finally, we compared the differences in the absorption signals. As a result, the absorption signals of *p*-fluorobenzyl radicals were found to be (65 ± 4)% of those of benzyl radicals. Since the absorption coefficient of benzyl radicals at 253 nm is known to be $\sigma_{\text{benzyl}}(253\text{ nm}) = 1.3 \times 10^{-16}$ cm^2 molecule^{-1},[21] in agreement with earlier data,[22,23] we could determine $\sigma_{p-\text{fluorobenzyl}}$ (at 253 nm) to be $(8.4 \pm 1.0) \times 10^{-17}$ cm^2 molecule^{-1}. Absorption coefficients of *p*-fluorobenzyl radicals were then scaled to the value at 253 nm. The resulting $\sigma_{p-\text{fluorobenzyl}}$ (λ, 300 K) are shown in Figure 2 and summarized in Table 2.

The absorption coefficients $\sigma_{p-\text{fluorobenzyl}}$ were found to be only weakly dependent on the pressure and the temperature. We checked if there was any influence of the pressure and temperature dependence of $\sigma_{p-\text{fluorobenzyl}}$ on our evaluation of k_1. First, in Figure 3A, we kept a constant ratio of [*p*-fluorobenzyl]$_0$/[CO_2] at different CO_2 pressures between 10 and 50 bar. The maximum absorption value of *p*-fluorobenzyl radicals at $t = 0$ as a function of CO_2 pressure was found to be linear, indicating no complications by solvent-induced changes of the absorption coefficients. Second, in Figure 3B, the absorption signals of *p*-fluorobenzyl radicals at 253 nm were measured at different temperatures between 255 and 420 K. The maximum

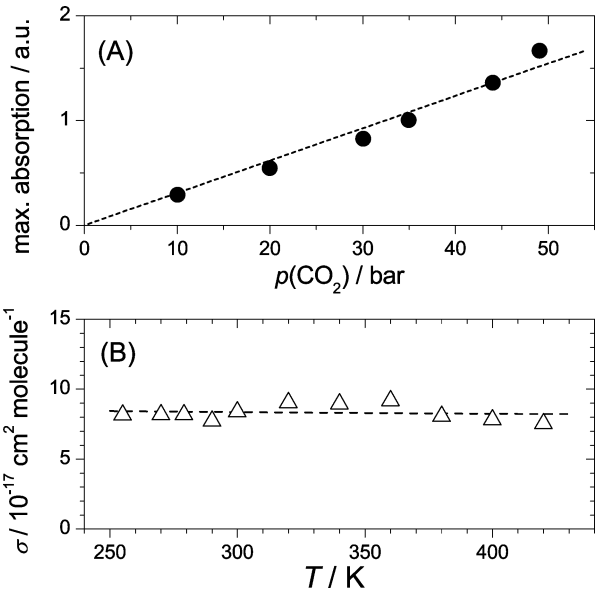

Figure 3. Pressure and temperature dependence of the absorption coefficient σ of *p*-fluorobenzyl radicals. (A) Maximum absorption of *p*-fluorobenzyl radicals at 253 nm at different CO_2 pressures with constant ratio $[Cl_2]/[CO_2] = 4 \times 10^{-5}$. (B) Calibrated values σ at 253 nm over the range 255−420 K.

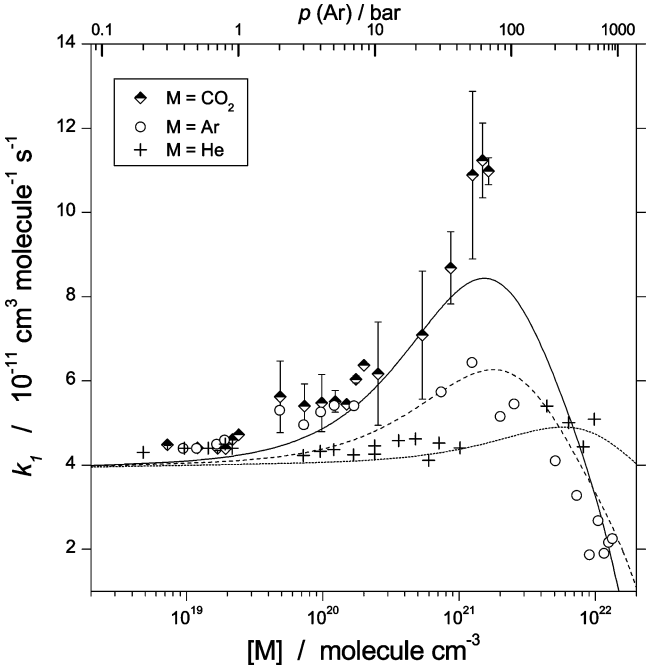

Figure 4. Recombination rate constant k_1 in helium (+), argon (○) and CO_2 (half-solid diamond) at 300 K. Error bars for CO_2 indicate the experimental scattering. Lines = rate constants for recombination of unsubstituted benzyl radicals in helium (···), argon (- - -) and CO_2 (—) from ref 16, given for comparison.

absorption coefficients at 253 nm showed only a weak temperature dependence expressed as

$$\sigma_{p-\text{fluorobenzyl}}(253\text{ nm}) = (8.4 \pm 0.4) \times 10^{-17}(T/300\text{ K})^{-0.05}\text{ cm}^2\text{ molecule}^{-1} \quad (4)$$

From this we could estimate that errors in $\sigma_{p-\text{fluorobenzyl}}(\lambda,T)$ could have caused, at most, 5% error in the measured k_1.

3.3. *P* and *T* Dependence of k_1. The observed pressure dependences of k_1 at 300 K are shown in Figure 4. At pressures between 200 and 900 mbar, pressure- and bath-gas-independent

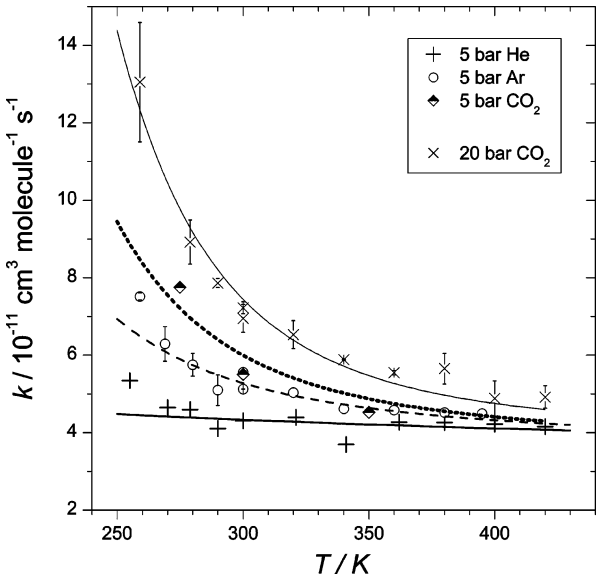

Figure 5. Temperature dependence of k_1 near 5 bar of helium (+), argon (○), and CO_2 (half-solid diamond) and near 20 bar CO_2 (×). Lines are from modeling in section 4.2.

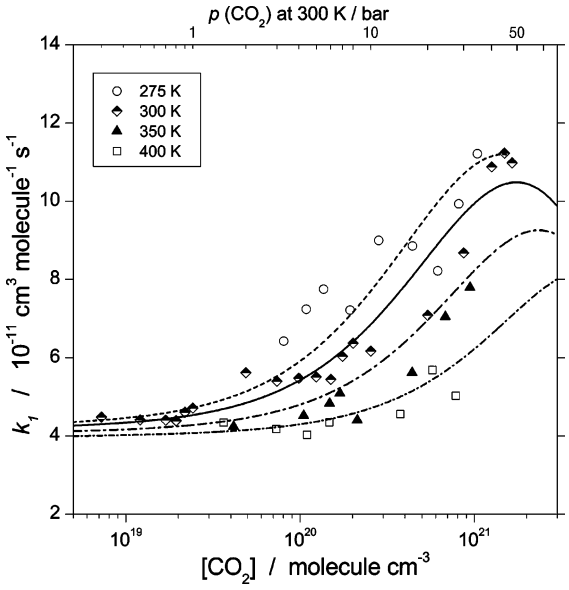

Figure 6. Density dependence of the combination rate constant k_1 in CO_2 at different temperatures. Lines from a fit in terms of the radical-complex mechanism, see text.

constant values of k_1 were observed from which we could derive limiting high-pressure rate constants of the energy-transfer mechanism, $k_{1,\infty}^{ET}(300\ K) = (4.3 \pm 0.5) \times 10^{-11}$ cm^3 molecule^{-1} s^{-1} (the error limits represent mostly the scatter of the data, and possible systematic errors present in the experiments are probably small; see the Experimental Section). In He, these k_1 values remained constant at pressures up to about 80 bar. In contrast, in the bath gases Ar and CO_2, at pressures of about 5 bar a further gradual increase of k_1 was already observed, until the increase slowed at densities where the influence of diffusion control sets in. As seen in Figure 4, the magnitude of this enhancement was dependent on the bath gas, increasing in the order He < Ar < CO_2. For comparison with our earlier results on the recombination of unsubstituted benzyl radicals,[16] we have added three lines in Figure 4 representing the pressure dependence of benzyl recombination in He, Ar and CO_2. The similarity with the present results on *p*-fluorobenzyl radicals is obvious. Only a slightly earlier onset of the enhancement of the k_1 values with a slightly larger magnitude was observed here.

We also measured the temperature dependence of $k_{1,\infty}^{ET}$ in He at 5 bar such as shown in Figure 5. Only a modest temperature dependence of $k_{1,\infty}^{ET}$ was observed over the temperature range 255−420 K. In contrast, at this pressure, the enhancement of the k_1 values was clearly taking place at lower temperatures in Ar and even more significantly in CO_2. At temperatures near 400 K, at this pressure, bath gas-independent kinetics was approached again and the k_1 values in Ar and CO_2 were reaching the same value as in He. The results in He (5 bar), therefore, allow one to determine safely the temperature dependence of $k_{1,\infty}^{ET}$. The resulting temperature dependence of $k_{1,\infty}^{ET}$ over the temperature range 255−420 K is expressed by

$$k_{1,\infty}^{ET} = (4.3 \pm 0.5) \times 10^{-11}(T/300\ K)^{-0.2}\ cm^3\ molecule^{-1}\ s^{-1} \quad (5)$$

The distinct temperature dependence of k_1 enhancement over the full pressure range was documented in CO_2 by measurements at 275, 300, 350, and 400 K. The results are shown in Figure 6. The most pronounced enhancement of k_1 was observed at 275 K and the strong decrease of the phenomenon with increasing temperature is documented again. In the following, we interpret these experimental observations in the framework of the radical-complex mechanism.

4. Discussion

4.1. Effect of Fluorine-Substitution of Benzyl-Type Radicals on k_1. Our current results show that the recombination kinetics as well as the UV spectroscopic properties of *p*-fluorobenzyl radicals do not significantly differ from those of benzyl radicals. The pressure-independent rate constant of the energy-transfer mechanism $k_{1,\infty}^{ET}$ of *p*-fluorobenzyl radicals is indeed very similar to the corresponding value for benzyl radicals of $k_\infty^{ET} = (4.1 \pm 0.3) \times 10^{-11}(T/300\ K)^{-0.3}$ cm^3 molecule^{-1} s^{-1}.[16] Compared to benzyl radicals,[21] the maximum of the *p*-fluorobenzyl absorption around 255 nm (Figure 2) is shifted to the red by only about 3 nm.

An insensitivity of recombination rate constants to the type and the position of substituents at the benzene ring has also been observed in gas-phase studies[9,10] of the combination of several benzyl-type radicals (benzyl, *p*-, *m*-, and *o*-fluorobenzyl, and *p*-, *m*-, and *o*-methylbenzyl). The rate constants for the combination of O_2 with benzyl, *p*-fluorobenzyl, and *p*-methylbenzyl radicals in liquid hexane were also identical, but smaller values were found for other substituted benzyl radicals.[24]

The enhancement of k_1 beyond the $k_{1,\infty}^{ET}$ value in the case of *p*-fluorobenzyl radicals, which was observed in the present work, qualitatively resembles that of benzyl radicals (see Figure 4). Quantitatively, however, its onset is observed to occur earlier for *p*-fluorobenzyl radicals (already at ∼5 bar) than for benzyl radicals (∼10 bar). Furthermore, the degree of enhancement of k_1 at high pressures is somewhat larger for *p*-fluorobenzyl radicals. In the following, we compare $k_{1,\infty}^{ET}$ with theoretical calculations. After that we will try to explain the enhancement of k_1 at high densities within the framework of the radical-complex mechanism.

4.2. Limiting High-Pressure Rate Constants in the ET Mechanism. An analysis of $k_{1,\infty}^{ET}$ in terms of unimolecular rate theory is a prerequisite for the analysis of the enhancement of k_1 within the radical-complex mechanism. No accurate ab initio potentials for reaction 1 are currently available which would allow for a quantitative interpretation of $k_{1,\infty}^{ET}$. We, therefore,

estimate $k_{1,\infty}^{ET}$ on the basis of statistical adiabatic channel/classical trajectory (SACM/CT) calculations for "standard" Morse potentials such as described in refs 25 and 26 for "linear + linear → nonlinear" reaction systems where the adduct angle corresponds to that of 1,2-bis(4-fluorophenyl)ethane.

We start by estimating the upper limit of $k_{1,\infty}^{ET}$ given by phase space theory, $k_{1,\infty}^{ET,PST}$, corresponding to the case of a fully isotropic interaction potential between the radicals. This rate constant is given by

$$k_{1,\infty}^{ET,PST} = \sqrt{\frac{8\pi kT}{\mu}}\frac{f}{\beta^2}\alpha_{spin}Y(T) \qquad (6)$$

with μ the reduced mass of the two reactants, the Morse parameter β of the interaction potential, the spin-statistical factor $\alpha_{spin} = {}^1/_4$, and the stoichiometric factor $f = 0.5$ for recombination of two identical reactants. An estimate of the reduced cross-section[25,26] $Y(T) = -31.153 - 18.158\ X(T) + 0.8685\ X(T)^2 = 426.0$ is evaluated from $X(T) = \ln(kT/D_0) + 4 - \beta r_e = -13.3$, where the center-of-mass equilibrium distance of the reactants in the adduct is $r_e = 6.3$ Å, as obtained from structural optimization on the B3LYP level with a 6-31G(d,p) basis set;[27] a bond dissociation energy $D_0 = 260.7$ kJ mol^{-1} ($D_0/hc = 2.18 \times 10^4$ cm^{-1}) was estimated by $D_0 = 2E_{min}$(*p*-fluorobenzyl radical) − E_{min}(1,2-bis(4-fluorophenyl)ethane), with E_{min} being the minimum energy of the respective optimized structures at the B3LYP level with a 6-31G(d,p) basis set.[27] This leads to a Morse parameter $\beta \approx 2.0$ Å^{-1} from the expression

$$\beta = 2\pi hc\nu_{C-C_{str}}\sqrt{\mu_{C-C}/2D_0} \qquad (7)$$

and a vibrational frequency $\nu_{C-C_{str}} = 991$ cm^{-1} of the C−C stretching mode. With these values, eq 6 results in

$$k_{1,\infty}^{ET,\,PST} = 1.4 \times 10^{-10}(T/300\ \text{K})^{+0.42}\ \text{cm}^3\,\text{molecule}^{-1}\,\text{s}^{-1} \qquad (8)$$

The difference between this value and the experimental $k_{1,\infty}^{ET}$ is attributed to consider the anisotropy of the potential. It is represented by the rigidity factor, f_{rigid}, which is the ratio of $k_{1,\infty}^{ET}/k_{1,\infty}^{ET,PST}$. The ratio between the experimental results of eq 5 and the PST value from eq 8 determines an experimental rigidity factor

$$f_{rigid}^{exp} \approx 0.31(T/300\ \text{K})^{-0.6} \qquad (9)$$

In the absence of a higher quality potential energy surface, a theoretical calculations of f_{rigid} is presently not possible. However, we use the methods of refs 25 and 26 for a rationalization of f_{rigid}^{exp} at 300 K. Following refs 25 and 26, we fit an α/β parameter, which then characterizes the anisotropy of the potential. With this result we can calculate the temperature dependence of f_{rigid}^{theory}. In this way, $f_{rigid}^{exp}(300\ \text{K}) = 0.31$ is found to correspond to $\alpha/\beta = 0.69$ and leading to a predicted temperature dependence

$$f_{rigid}^{exp} \approx 0.31\ (T/300\ \text{K})^{-0.5} \qquad (10)$$

which is in good agreement with the experimental result from eq 9. Combining eqs 8 and 10 results in

$$k_{1,\infty}^{ET,theory} = 4.3 \times 10^{-11}(T/300\ \text{K})^{-0.1}\ \text{cm}^3\,\text{molecule}^{-1}\,\text{s}^{-1} \qquad (11)$$

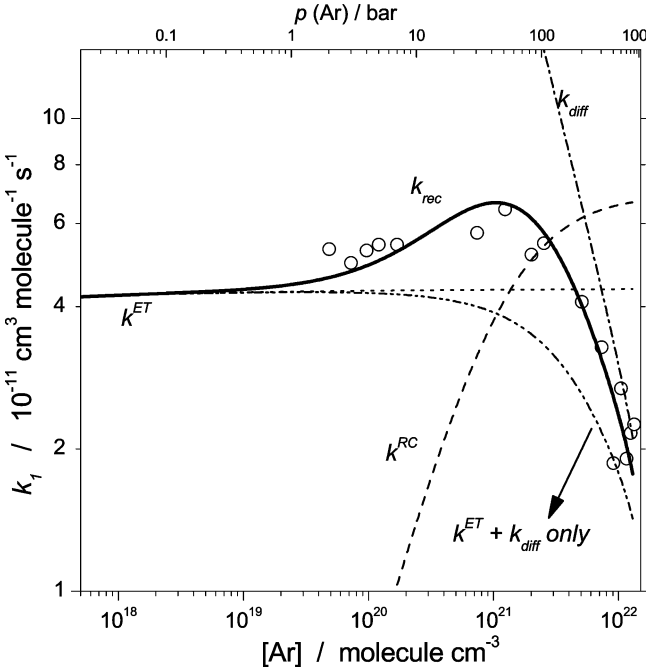

Figure 7. Density dependence of the combination rate constant k_1 in the bath gas argon at 300 K. (...): k^{ET} from the energy-transfer mechanism; (−•−): limiting diffusion-controlled rate constants; (- - -): k^{RC} from the radical-complex mechanism; (−••−): resulting rate constants without k^{RC}; and (—): resulting rate constants including k^{RC}. Fitting parameters used in this calculation are summarized in Table 3.

where the calculated temperature dependence agrees well with the experimental result from eq 5.

4.3. Transition to Diffusion-Controlled Kinetics. The decrease of k_1 at the highest pressures of Figure 4 can be attributed to the growing influence of diffusion control. Recombination rate constants (k_{rec}) in the gas−liquid transition range can be approximated by the following relationship:[28]

$$k_{rec} = k_{diff}[k_{rec}^{g}/(k_{rec}^{g} + k_{diff})] \qquad (12)$$

with $k_{diff} = 4\pi\alpha_{spin}(M)DR$. k_{diff} is the value of k_1 at full diffusion control of the reaction, while k_{rec}^{g} is the hypothetical value of the combination rate constant in the absence of diffusion control. As above we use a constant $\alpha_{spin}(M) = {}^1/_4$ (see ref 16 for more detailed explanations). D is the diffusion coefficient of the recombining radicals in the bath gas and estimated by the semiempirical method suggested in refs 29 and 30. This approach is based on the rough hard sphere theory which treats the intermolecular interaction between solute and solvent as being of Lennard-Jones (LJ) type. Here $\sigma_{LJ} = 5.95$ Å and $\epsilon_{LJ}/k = 386$ K were used for *p*-fluorobenzyl radicals, which were estimated following the method suggested by Tee et al.[31] The contact distance R is related to the thermally averaged capture cross section $\langle\sigma\rangle$ of two radicals in the "high-pressure limit" within the energy-transfer mechanism:[17]

$$R = \sqrt{\frac{\langle\sigma\rangle}{\pi}} = \left(\frac{1}{\alpha_{spin}(M)\pi f}k_{\infty}^{ET}\sqrt{\frac{\pi\mu}{8kT}}\right)^{1/2} \qquad (13)$$

This leads to $R = 5.7$ Å.

Figures 7 and 8 show the calculated rate constants k_{diff} and k^{ET} according to the energy-transfer mechanism and the combination of k_{diff} and k^{ET} by eq 12, first assuming that k_{rec}^{g} is given by k^{ET}. Diffusion control in the high-density region is

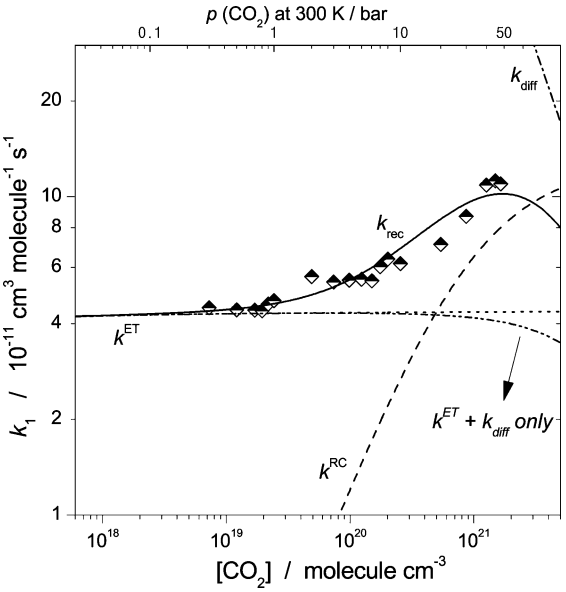

Figure 8. Plot as in Figure 7, but at 300 K in CO_2.

clearly limiting the kinetics at the highest pressures. However, our experimental data for k_1 at pressures of about 5−300 bar in the bath gas Ar and of about 3−50 bar in CO_2 clearly differ from a smooth transition between energy-transfer and diffusion-controlled kinetics (marked: "k^{ET}+k_{diff} only" in Figures 7 and 8). In the next section, we discuss the radical-complex mechanism (denoted by k^{RC}) as being responsible for the enhancement of k_1.

4.4. Contribution k^{RC} from the Radical-Complex Mechanism. The enhancement of k_1 by a contribution from the RC mechanism can be identified and quantified much better for the recombination of large radicals than for small radicals because in the former case the ET mechanism is fully in the "high-pressure" limit below 1 or even 0.1 bar.[16,17] Additional contributions to k_1 are then easily identified and not disturbed by underlying falloff contributions from the ET-mechanism. These additional contributions k^{RC} to k_1 shown in Figures 7 and 8 are the central, new information in this work. In the following, we try to provide a quantitative interpretation of k^{RC} in analogy to that in ref 16.

We start from looking at the combined ET- and RC-mechanism for the *p*-fluorobenzyl radical combination:

$$\mathrm{A} + \mathrm{A} \rightleftarrows \mathrm{A_2}^* \quad k_a, k_{-a} \tag{14}$$

$$\mathrm{A_2}^* + \mathrm{M} \rightarrow \mathrm{A_2} + \mathrm{M} \quad k_b$$

$$\mathrm{A} + \mathrm{M} \rightleftarrows \mathrm{AM} \quad k_c, k_{-c}, K_{eq} \tag{15}$$

$$\mathrm{AM} + \mathrm{A} \rightarrow \mathrm{A_2} + \mathrm{M} \quad k_{AM+A}$$

$$\mathrm{AM} + \mathrm{AM} \rightarrow \mathrm{A_2} + 2\mathrm{M} \quad k_{AM+AM}$$

The combined rate constant from both mechanisms, neglecting diffusion control, is then represented by

$$k_{1,rec} = k_1^{ET} + k_1^{RC} = \frac{k_{1,\infty}^{ET} k_{1,0}^{ET}[M]}{k_{1,\infty}^{ET} + k_{1,0}^{ET}[M]} F_c + \frac{K_{eq} k_{AM+A}[M] + K_{eq}^2 k_{AM+AM}[M]^2}{(1 + K_{eq}[M])^2} \tag{16}$$

F_c denotes the broadening factor of the falloff curve in the energy-transfer mechanism. The equilibrium constant K_{eq} contained in k_1^{RC} was estimated using the improved Bunker−Davidson expression by Schwarzer and Teubner.[32] The values of K_{eq} at 300 K are in the range $(0.6-10) \times 10^{-22}$ cm^3 molecule^{-1} and show an increasing order of K_{eq}(He) < K_{eq}(Ar) < K_{eq}(CO_2); see Table 3. k_{AM+A} controls the increase while k_{AM+AM} describes the limiting high-pressure rate constant in the radical-complex mechanism at the saturation of the reactive AM concentration. k_{AM+A} and k_{AM+AM} can both be determined independently. The solid lines in Figures 7 and 8 account for the sum of contributions from the ET mechanism, from the RC mechanism and from diffusion-controlled kinetics according to eq 12.

Table 3 summarizes the resulting fitting parameters of k_{AM+A} and k_{AM+AM} for M = He, Ar, and CO_2, and includes the previous results for A = benzyl radicals for comparison.[16] Several points should be noted: (i) for both benzyl and *p*-fluorobenzyl radicals, the fits of the experiments suggest that values of k_{AM+A} and k_{AM+AM} are larger than k_{A+A} (= $k_{1,\infty}^{ET}$); (ii) k_{AM+A} and k_{AM+AM} increase in the order He < N_2 ≈ Ar < CO_2; (iii) values of k_{AM+A} and k_{AM+AM} in all bath gases are rather similar for both benzyl and *p*-fluorobenzyl radicals, but systematically somewhat larger values of k_{AM+A} and k_{AM+AM} were measured for the *p*-fluorobenzyl radicals than for benzyl radicals. For a detailed theoretical understanding of these trends, one would need ab initio calculations of the AM + A and AM + AM potentials and CT calculations of capture on such potentials, which are not currently available. As pointed out in our earlier studies,[16,17] the analysis of the rigidity factors may provide an explanation of the observed enhancement of k_{AM+AM} above the value of k_{A+A}. The presence of a van der Waals complex partner M could possibly shield and reduce the anisotropy of the valence potential between A and A which then could result in larger rigidity factors and subsequently larger rate constants for k_{AM+AM} compared to k_{A+A}.[16,17] The experimental rigidity factor f_{rigid}^{exp} in k_{AM+AM} was indeed found to increase in the order He (≈ 0.35) < Ar (≈ 0.41) < CO_2 (≈ 0.66) and was in any case larger than f_{rigid}^{exp}in k_{A+A} (≈ 0.31). We estimated f_{rigid}^{exp} in k_{AM+AM} with $k_{AM+AM}^{PST} = 1.9 \times 10^{-10}$ cm^3 molecule^{-1} s^{-1} obtained by the same methods described in section 4.2. k_{AM+AM}^{PST} is found to be very similar to $k_{A+A}^{PST} = 1.4 \times 10^{-10}$ cm^3 molecule^{-1} s^{-1}. In this calculation the distance of the center of mass of the two reactants, r_e, AM + AM = 9.3 Å, and their dissociation energies were estimated following structural optimization at the B3LYP level with a 6-31G(d,p) basis set.[27] In addition, we assumed that the dissociation energies $D_{0,A+A} \approx D_{0,AM+AM} = 2.18 \times 10^4$ h c cm^{-1}, and that changes in the vibrational frequencies in the C−C stretching modes, $\nu_{C-C_{str}}$, for A+A and AM+AM, are negligible. f_{rigid}^{exp} in k_{AM+A} only showed small variations but was still increasing in the order He (≈ 0.34) < Ar (≈ 0.36) < CO_2 (≈ 0.37).

k^{RC} was also investigated in the bath gas CO_2 at the temperatures 275, 300, 350, and 400 K. Figure 6 shows a fit to our experimental data; see Table 3 for the fitted values. The observation of a much stronger negative temperature dependence of k_1 at high pressure than observed for the ET mechanism, see eq 5, supports our hypothesis of a contribution from the RC mechanism. The larger enhancement of k_1 at lower temperatures is mainly due to the increase of the equilibrium constants[32]

$$K_{eq}(T) = 1.0 \times 10^{-21} (T/300\ \mathrm{K})^{-3.5}\ \mathrm{cm^3\ molecule^{-1}} \quad (250 < T < 450\ \mathrm{K}) \tag{17}$$

TABLE 3: Kinetic Data Used for the Characterization of the Radical-Complex Mechanism

A	M	*T*/K	k_{A+A} (=$k_{1,\infty}^{ET}$)[a]	K_{eq}(AM)[b]	k_{AM+A}[a]	k_{AM+AM}[a]	ref
p-fluorobenzyl	He	300	4.3×10^{-11}	6.4×10^{-23}	9.1×10^{-11}	6.9×10^{-11}	this work
	Ar			5.6×10^{-22}	1.0×10^{-10}	8.1×10^{-11}	this work
	CO_2			1.0×10^{-21}	1.0×10^{-10}	13.8×10^{-11}	this work
	CO_2	275	4.4×10^{-11}	1.2×10^{-21}	1.1×10^{-10}	14.0×10^{-11}	this work
		350	4.2×10^{-11}	7.9×10^{-22}	9.9×10^{-11}	13.3×10^{-11}	
		400	4.1×10^{-11}	6.4×10^{-22}	9.7×10^{-11}	12.9×10^{-11}	
benzyl	He	300	4.1×10^{-11}	6.6×10^{-23}	8.1×10^{-11}	5.6×10^{-11}	16
	Ar			5.8×10^{-22}	8.4×10^{-11}	7.5×10^{-11}	16
	CO_2			1.1×10^{-21}	8.9×10^{-11}	11.9×10^{-11}	16

[a] Rate constant, given in cm^3 $molecule^{-1}$ s^{-1}. [b] Equilibrium constant, given in cm^3 $molecule^{-1}$.

and much less to the weak temperature dependence of the rate constants k_{AM+A} and k_{AM+AM}, see eq 16 and Table 3:

$$k_{AM+AM}^{exp}(T) = 1.3 \times 10^{-10}(T/300\ K)^{-0.3}\ cm^3\,molecule^{-1}\,s^{-1} \quad (18)$$

$$k_{AM+A}^{exp}(T) = 1.0 \times 10^{-11}(T/300\ K)^{-0.3}\ cm^3\,molecule^{-1}\,s^{-1} \quad (19)$$

By comparing these values with k_{AM+AM}^{PST} and k_{AM+A}^{PST}, respectively, the experimental temperature-dependent rigidity factors are given by $f_{rigid,AM+AM}^{exp}(T) = 0.66(T/300\ K)^{-0.6}$ and $f_{rigid,AM+A}^{exp}(T) = 0.36(T/300\ K)^{-0.5}$. We found good agreements of these results of $k_{AM+AM}^{exp}(T)$ and $f_{rigid,AM+AM}^{exp}(T)$ with theoretical estimates obtained following the methods described in section 4.2. For this, we characterized the interaction between two AM (*p*-fluorobenzyl + CO_2) by a Morse potential with $r_{e,AM+AM} = 9.3$ Å and fitted $\alpha/\beta \approx 0.69$ from the value of f_{rigid} at 300 K. This gives us a prediction of $f_{rigid,AM+AM}^{theory} \approx 0.67(T/300\ K)^{-0.5}$ which is very close to our experimental value. A theoretical estimate of $k_{AM+AM}^{theory}(T) = 1.2 \times 10^{-10}(T/300\ K)^{-0.1}$ cm^3 $molecule^{-1}$ s^{-1} is again in agreement with the experimental result from eq 18.

5. Conclusions

Pressure and temperature dependences of the recombination reaction of *p*-fluorobenzyl radicals have been investigated over the pressure range of 0.2−800 bar at temperatures of 255−420 K in the bath gases helium, argon and CO_2. Pressure and bath-gas independent rate constants below 0.9 bar in CO_2 and Ar and below 40 bar in He allowed for a direct determination of the limiting "high-pressure" rate constant of the conventional energy-transfer mechanism for recombination reactions: $k_{1,\infty}^{ET} = (4.3 \pm 0.5) \times 10^{-11}\ (T/300\ K)^{-0.2}$ cm^3 $molecule^{-1}$ s^{-1}. The value was analyzed in terms of SACM/CT theory. Above about 5 bar the radical recombination rates k_1 show a pressure, temperature and bath-gas dependent increase in the range where the conventional mechanism of recombination predicts a pressure-independent value $k_{1,\infty}^{ET}$. Our observations of such enhanced rate constants of the free radical combination and their marked dependence on temperature and the nature of the solvent are consistently explained as kinetic contribution of the radical-complex mechanism of recombination, involving radical−solvent van der Waals complexes. There was no significant effect of the fluorine-substitution of the benzyl ring on k_1 values, and only a slightly earlier onset and a slightly greater degree of the enhancement of k_1 values at high pressures were found in the recombination of *p*-fluorobenzyl radicals compared to that of benzyl radicals. The present results on *p*-fluorobenzyl radicals recombination are another example for the "unexpected" type of pressure dependence, in addition to those recently already reported for the combination reactions of CCl_3 radicals, of CCl_3 with Br[17] as well as of benzyl radicals.[16] They support the expectation that similar phenomena caused by the increasing rate of the radical-complex mechanism may be rather general for radical recombination in the gas−liquid transition region. A more detailed analysis of the analogous situation for large radical systems like biphenyl, as well as combination reactions of smaller radicals such as O + O_2 and ClO + ClO, especially at low temperatures, is underway.

Acknowledgment. Financial support by the Alexander von Humboldt Foundation ("Sofja Kovalevskaja Program") as well as helpful discussions with V. G. Ushakov and T. Lenzer are gratefully acknowledged.

References and Notes

(1) Kajimoto, O. *Chem. Rev.* **1999**, *99*, 355.
(2) Brennecke, J.; Chateauneuf, J. E. *Chem. Rev.* **1999**, *99*, 433.
(3) Rabinowitch, E. *Trans. Faraday Soc.* **1937**, *33*, 283.
(4) Porter, G.; Smith, J. A. *Proc. Royal Soc. London, A.* **1961**, *261*, 28.
(5) Hippler, H.; Luther, K.; Troe, J. *Ber. Bunsen-Ges. Phys. Chem.* **1973**, *77*, 1020.
(6) Hippler, H.; Rahn, R.; Troe, J. *J. Chem. Phys.* **1990**, *93*, 6560.
(7) Luther, K.; Oum, K.; Troe, J. *Phys. Chem. Chem. Phys.* **2005**, *7*, 2764.
(8) Hamon, S.; Speck, T.; Mitchell, J. B. A.; Rowe, B. R.; Troe, J. *J. Chem. Phys.* **2002**, *117*, 2557.
(9) Goumri, A.; Pauwels, J. F.; Sawerysyn, J. P.; Devolder, P. *Chem. Phys. Lett.* **1990**, *171*, 303.
(10) Goumri, A.; Elmaimouni, L.; Sawerysyn, J. P.; Devolder, P. *J. Phys. Chem.* **1992**, *96*, 5395.
(11) Bindley, T. F.; Watts, A. T.; Walker, S. *Trans. Faraday Soc.* **1964**, *60*, 1.
(12) Cossart-Magos, C.; Cossart, D. *Mol. Phys.* **1988**, *65*, 627.
(13) Charlton, T. R.; Thrush, B. A. *Chem. Phys. Lett.* **1986**, *125*, 547.
(14) Fukushima, M.; Obi, K. *J. Chem. Phys.* **1990**, *93*, 8488.
(15) Lee, S. K.; Baek, D. Y. *Chem. Phys. Lett.* **1999**, *301*, 407.
(16) Luther, K.; Oum, K.; Sekiguchi, K.; Troe, J. *Phys. Chem. Chem. Phys.* **2004**, *6*, 4133.
(17) Oum, K.; Luther, K.; Troe, J. *J. Phys. Chem. A* **2004**, *108*, 2690.
(18) Oum, K.; Sekiguchi, K.; Luther, K.; Troe, J. *Phys. Chem. Chem. Phys.* **2003**, *5*, 2931.
(19) Hoffbauer, M. A.; Hudgens, J. W. *J. Phys. Chem.* **1985**, *89*, 5152.
(20) Nelson, H. H.; McDonald, J. R. *J. Phys. Chem.* **1982**, *86*, 1242.
(21) Fay, N. Ph.D. Thesis, Göttingen University, 1997.
(22) Ikeda, N.; Nakashima, N.; Yoshihara, K. *J. Phys. Chem.* **1984**, *88*, 5803.
(23) Markert, F.; Pagsberg, P. *Chem. Phys. Lett.* **1993**, *209*, 445.
(24) Tokumura, K.; Nosaka, H.; Ozaki, T. *Chem. Phys. Lett.* **1990**, *169*, 321.
(25) Maergoiz, A. I.; Nikitin, E. E.; Troe, J.; Ushakov, V. G. *J. Chem. Phys.* **1998**, *108*, 5265.
(26) Maergoiz, A. I.; Nikitin, E. E.; Troe, J.; Ushakov, V. G. *J. Chem. Phys.* **1998**, *108*, 9987.
(27) Frisch, M. J.; Trucks, G. W.; Schlegel, H. B.; Scuseria, G. E.; Robb, M. A.; Cheeseman, J. R.; Montgomery, J. A., Jr.; Burant, J. C.; Millam, J. M.; Iyengar, S. S.; Tomasi, J.; Barone, V.; Mennucci, B.; Cossi, M.; Scalmani, G.; Rega, N.; Petersson, G. A.; Nakatsuji, H.; Hada, M.; Ehara, M.; Toyota, K.; Fukuda, R.; Hasegawa, J.; Ishida, M.; Nakajima, T.; Honda, Y.; Kitao, O.; Nakai, H.; Klene, M.; Li, J. E. K. X.; Hratchian, H. P.; Cross,

J. B.; Adamo, C.; Jaramillo, J.; Gomperts, R.; Stratmann, R. E.; Yazyev, O.; Austin, A. J.; Cammi, R.; Pomelli, C.; Ochterski, J. W.; Ayala, P. Y.; Morokuma, K.; Voth, G. A.; Salvador, P.; Dannenberg, J. J.; Zakrzewski, V. G.; Dapprich, S.; Daniels, A. D.; Strain, M. C.; Farkas, O.; Malick, D. K.; Rabuck, A. D.; Raghavachari, K.; Foresman, J. B.; Ortiz, Q. C. J. V.; Baboul, A. G.; Clifford, S.; Cioslowski, J.; Stefanov, B. B.; Liu, G.; Liashenko, A.; Piskorz, P.; Komaromi, I.; Martin, R. L.; Fox, D. J.; Keith, T.; Al-Laham, M. A.; Peng, C. Y.; Nanayakkara, A.; Challacombe, M.; Gill, P. M. W.; Johnson, B.; Chen, W.; Wong, M. W.; Gonzalez, C.; Pople, J. A. Gaussian 03. Revision B.04 ed.; Gaussian Inc.: Pittsburgh, PA, 2003.

(28) Troe, J. *J. Phys. Chem.* **1986**, *90*, 357.

(29) Ruckenstein, E.; Liu, H. *Ind. Eng. Chem. Res.* **1997**, *36*, 3927.

(30) Liu, H.; Ruckenstein, E. *Ind. Eng. Chem. Res.* **1997**, *36*, 5488.

(31) Tee, L. S.; Gotoh, S.; Stewart, W. E. *Ind. Eng. Chem. Fundam.* **1966**, *5*, 356.

(32) Schwarzer, D.; Teubner, M. *J. Chem. Phys.* **2002**, *116*, 5680.